



# HHS Public Access

Author manuscript

*Arterioscler Thromb Vasc Biol.* Author manuscript; available in PMC 2021 May 01.

Published in final edited form as:

*Arterioscler Thromb Vasc Biol.* 2020 May ; 40(5): 1123–1134. doi:10.1161/ATVBAHA.119.313629.

## Whole-body atherosclerosis imaging by PET/MRI: from mice to non-human primates

**Claudia Calcagno, MD, PhD<sup>1,2</sup>, Carlos Pérez-Medina, PhD<sup>1,2,3</sup>, Willem J.M. Mulder, PhD<sup>1,2,4,5</sup>, Zahi A. Fayad, PhD<sup>1,2</sup>**

<sup>1</sup>BioMedical Engineering and Imaging Institute, Icahn School of Medicine at Mount Sinai, New York, USA <sup>2</sup>Department of Radiology, Icahn School of Medicine at Mount Sinai, New York, USA <sup>3</sup>Centro Nacional de Investigaciones Cardiovasculares (CNIC), Madrid, Spain <sup>4</sup>Department of Oncological Sciences, Icahn School of Medicine at Mount Sinai, New York, NY, USA <sup>5</sup>Laboratory of Chemical Biology, Department of Biomedical Engineering and Institute for Complex Molecular Systems, Eindhoven University of Technology, Eindhoven, The Netherlands

### Abstract

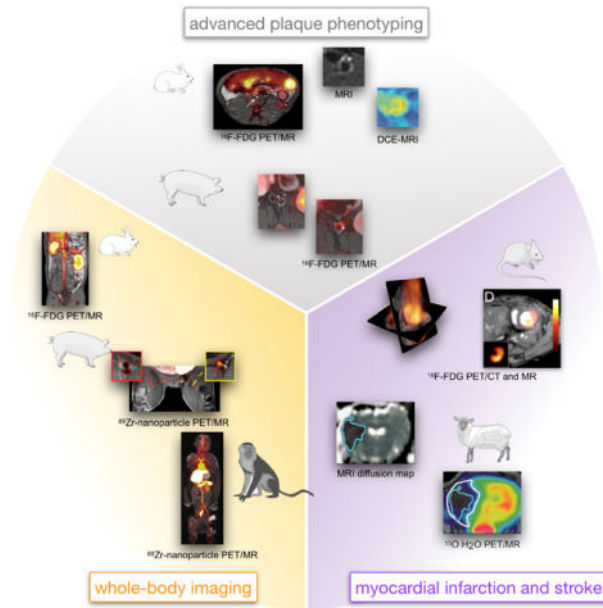
Cardiovascular disease due to atherosclerosis is still the main cause of morbidity and mortality worldwide. This disease is a complex systemic disorder arising from a network of pathological processes within the arterial vessel wall, and, outside of the vasculature, in the hematopoietic system and organs involved in metabolism. Recent years have seen tremendous efforts in the development and validation of quantitative imaging technologies for the non-invasive evaluation of patients with atherosclerotic cardiovascular disease. Specifically, the advent of combined positron emission tomography (PET) and magnetic resonance imaging (MRI) scanners has opened new exciting opportunities in cardiovascular imaging. In this review we will describe how combined PET/MRI scanners can be leveraged to evaluate atherosclerotic cardiovascular disease at the whole-body level, with specific focus on pre-clinical animal models of disease, from mouse to non-human primates. We will broadly describe 3 major areas of application: i) vascular imaging, for advanced atherosclerotic plaque phenotyping and evaluation of novel imaging tracers or therapeutic interventions; ii) assessment of the ischemic heart and brain; and iii) whole-body imaging of the hematopoietic system. Finally, we will provide insights on potential novel technical developments which may further increase the relevance of integrated PET/MRI in pre-clinical atherosclerosis studies.

### Graphical abstract

---

**Corresponding author:** Zahi A. Fayad, PhD, FAHA, FACC, FISMRM, Icahn School of Medicine at Mount Sinai, Professor Department of Radiology and Medicine (Cardiology), Director, BioMedical Engineering and Imaging Institute, Director, Cardiovascular Imaging Research, Vice chair for Research, Department of Radiology, One Gustave L. Levy Place, New York, NY, 10029, Phone: 212-824-8452, zahi.fayad@mssm.edu.

**Disclosure.** None



## Keywords

PET/MRI; atherosclerosis; cardiovascular disease; pre-clinical imaging

## Subject codes.

Animal Models of Human Disease; Inflammation; Magnetic Resonance Imaging (MRI); Nuclear Cardiology and PET; Atherosclerosis

Atherosclerosis, the underlying cause of many cardiovascular diseases, is a complex systemic disorder arising from a network of pathological processes within the arterial vessel wall, and, outside of the vasculature, in the hematopoietic system<sup>1, 2</sup> and organs involved in metabolism. Recent years have seen tremendous efforts in the development and validation of non-invasive technologies based on positron emission tomography (PET) and magnetic resonance imaging (MRI), to enable the quantitative multi-parametric and multi-modality evaluation of cardiovascular disease at the whole-body level<sup>2</sup>.

The information provided by cardiovascular PET and MRI is very different, yet highly complementary<sup>3</sup> (Table 1). Positron emission tomography (PET) is a quantitative nuclear imaging technique that allows the visualization of radioisotopes and is mostly applied to investigate tissue metabolic and physiological state at the molecular level with high sensitivity<sup>4</sup>. <sup>18</sup>F-labeled fluorodeoxyglucose (FDG) is the most widely used and validated PET tracer in clinical and pre-clinical atherosclerosis research<sup>4</sup>. <sup>18</sup>F-FDG is a radiolabeled glucose analog that is internalized, but not metabolized, by metabolically active cells<sup>4</sup>. In the arterial vessel wall, <sup>18</sup>F-FDG is a well validated surrogate quantitative marker of vessel wall inflammation (plaque macrophage content)<sup>5-7</sup>, a hallmark of vulnerable plaques at high risk for causing myocardial infarction and stroke. In the infarcted heart, <sup>18</sup>F-FDG PET can be used to assess cardiomyocyte viability in the remote myocardium<sup>8</sup>, or, alternatively, active

inflammation in the infarct itself<sup>9</sup>, both important markers of patients' prognosis. In agreement with recent mouse atherosclerosis studies<sup>10</sup>, clinical studies show that <sup>18</sup>F-FDG PET can also inform on increased metabolic activity in hematopoietic organs (bone marrow and spleen) and in the aortic arch in patients with recent myocardial infarction<sup>11, 12</sup>, suggesting that this technique is well positioned to provide a systems-level evaluation of myelopoiesis in cardiovascular disease. PET imaging has also been successfully applied in multiple clinical and pre-clinical atherosclerosis trials, as a surrogate endpoint of anti-inflammatory drug efficacy using <sup>18</sup>F-FDG, or to track the whole-body distribution (kinetics) of novel therapeutics based on radiolabeled antibodies and nanomedicines. In this setting, this technique consistently demonstrated reduction of <sup>18</sup>F-FDG uptake and plaque inflammation after treatment with standard-of-care statins<sup>13</sup>, but variable results with other anti-inflammatory compounds. To surpass these challenges, PET tracers other than <sup>18</sup>F-FDG are also being actively explored to investigate other processes involved in atherogenesis<sup>14</sup> and offer a more specific quantification of inflammatory cells.

Separately, MRI-based methods have been developed and widely employed over the years to probe several parameters related to atherogenesis and its local and systemic consequences. MRI acquisitions with one preferred image weighting (T1, T2 or proton density [PD]) can be used to assess atherosclerotic plaque area, vessel wall thickening and overall disease burden in a specific vessel<sup>15</sup>. The combination of MR images with different weightings with or without gadolinium (Gd) enhancement, or the use of more quantitative T1 and T2 relaxation mapping, allow the identification of different plaque components related to vulnerability, such as presence of lipid core and fibrous cap<sup>15</sup>. Other quantitative techniques, such as dynamic contrast enhanced (DCE) MRI, can be used to measure endothelial permeability and neovascularization in the vessel wall, infarcted heart and hematopoietic organs, parameters related to plaque inflammation and vulnerability, myocardial damage, and immune cell migration<sup>16</sup>. Molecular imaging approaches, such as iron oxide-enhanced MRI, can offer valuable insights into the molecular and cellular makeup of vulnerable atherosclerotic plaques<sup>17</sup>.

Up to now, most atherosclerosis imaging studies using PET and MRI have probed only one or a few imaging parameters at a time, and separately focused either on the vasculature, the infarcted heart or brain, or hematopoietic organs. Furthermore, most studies have used only one imaging modality, either MRI or PET, or, at best, sequential acquisitions with both techniques. However, these approaches do not optimally take advantage of the complementary information provided by cardiovascular PET and MRI.

The advent of combined PET/MRI scanners opens new exciting opportunities in cardiovascular imaging<sup>3</sup>. Commonly, PET is acquired together with computed tomography (CT) on hybrid PET/CT scanners. However, CT provides only limited information on plaque burden and phenotype compared to MRI. Better than PET/CT, integrated PET/MRI effectively combines the highly sensitive, quantitative information from PET with the superior soft tissue contrast and multi-parametric evaluation allowed by MRI. Crucial to the success of cardiovascular PET/MRI has been the recent development of fully 3 dimensional (3D), high-resolution (0.6<sup>3</sup>-0.8<sup>3</sup> mm<sup>3</sup>) vascular MRI sequences with extended spatial coverage<sup>18-20</sup>. On integrated PET/MRI scanners, these 3D MRI acquisitions allow obtaining

information on plaque burden, composition and permeability/neovascularization that can be seamlessly co-registered with PET readouts of disease activity. Last but not least, compared to PET/CT, PET/MRI acquires these sophisticated metrics while lowering subjects' exposure to ionizing radiation. This feature facilitates longitudinal follow-up studies, which is relevant for long term monitoring of chronic diseases, such as atherosclerosis. Thanks to these advantages, several groups foresee that the use of cardiovascular PET/MRI may rapidly rise in the near future<sup>21</sup>.

In this review, we will focus on the specific strengths of PET/MRI for the whole-body multi-parametric evaluation of atherosclerotic cardiovascular disease in the pre-clinical arena, from mice to non-human primates. We will broadly describe 3 major areas of application: i) vascular imaging, for advanced atherosclerotic plaque phenotyping and evaluation of novel imaging tracers or therapeutic interventions; ii) assessment of the ischemic heart and brain; and iii) whole-body imaging of the hematopoietic system. *Finally, we will provide insights into the remaining challenges in using this multi-modality approach for atherosclerosis research, and potential novel technical developments which may further increase the relevance of integrated PET/MRI in pre-clinical atherosclerosis studies.*

## **Vascular PET/MRI for advanced plaque phenotyping and in drug development**

In the pre-clinical field, vascular imaging studies using sequential or combined PET/MRI have been conducted in small (mice, rats) and large (rabbit, swine) animal models of atherosclerosis. Studies in mice have often employed sequential acquisitions on separate PET/CT and MRI scanners, or, more rarely, combined PET/MRI systems consisting either of prototype PET inserts fitted for small animal MRI scanners, or standalone integrated solutions. Many of these studies have used high-field MRI to aid in the development and validation of novel PET atherosclerosis tracers developed to improve the detection of vulnerable plaques (such as <sup>64</sup>Cu-labeled soluble scavenger receptor (CD68-Fc) targeted to foam cells<sup>22</sup> and <sup>68</sup>Ga-labeled fucoidan targeted to P-selectin<sup>23</sup>). Using similar approaches, other studies in mice and rats have focused on the development of multimodal agents that can be detected by both MRI and PET to improve plaque characterization, such as <sup>64</sup>Cu-labeled Gd-bovine serum albumin (Gd-BSA) or cross-linked iron-oxides (CLIOs)<sup>24</sup>, and <sup>68</sup>Ga-labeled iron oxide nanoparticles<sup>25</sup>.

Vascular PET/MRI studies in large animals, such as atherosclerotic rabbits and pigs, have instead focused on improving plaque phenotyping and the assessment of therapeutic response using already available or novel PET tracers, combined with high-resolution multi-parametric MRI. Early rabbit studies used sequential <sup>18</sup>F-FDG PET/CT of plaque inflammation, MRI of plaque burden and DCE-MRI of permeability/neovascularization as separate non-invasive readouts of therapeutic efficacy of FDA-approved and novel anti-atherosclerotic compounds (such as atorvastatin<sup>7</sup>, glucocorticoid loaded liposomes<sup>26</sup>, liver X receptor [LXR] agonists<sup>7</sup>, pioglitazone<sup>6</sup>). The application of combined clinical PET/MRI scanners for imaging large animal models of cardiovascular disease is more recent, but has significant advantages, as large animal PET/MRI acquisition and analysis protocols are

translatable to humans. Among the first to use this approach, Millon et al.<sup>27</sup> used a clinical PET/MRI system consisting of two separate, but immediately adjacent, PET and MRI scanners (Philips 3T Achieva, Philips Healthcare Systems, Best, The Netherlands), to assess therapeutic response to a 6 months atorvastatin regimen (3 mg/Kg/day) plus switch to a chow diet in rabbits. Plaque inflammation was quantified with both <sup>18</sup>F-FDG PET and MRI with a novel ultrasmall iron oxide particle (P904, Guerbet, Paris, France). The authors found a reduction in plaque <sup>18</sup>F-FDG and iron oxide uptake after treatment, with good correlations between the two imaging readouts and histology ( $R^2 = 0.778$  and  $0.707$  respectively). Differently than previous studies employing PET/CT, no change in these parameters was found in the progression (control) group, kept on high fat diet. Using instead a fully combined PET/MRI scanner (Biograph mMR, Siemens Healthineers, Erlangen, Germany), we<sup>28</sup> evaluated the therapeutic efficacy of a novel leukotriene synthesis inhibitor in a rabbit atherosclerosis model. This more advanced setup allowed us to fully integrate the measurement of plaque inflammation by <sup>18</sup>F-FDG PET with high-resolution, 3 dimensional imaging of atherosclerosis burden (plaque area) by MRI and endothelial permeability/neovascularization by DCE-MRI across the whole rabbit infrarenal abdominal aorta. In addition to providing a more comprehensive evaluation of therapeutic efficacy, this integrated framework allowed exploring the correlations between these co-registered imaging metrics. This analysis revealed significant relationships between inflammation by <sup>18</sup>F-FDG PET, permeability/neovascularization by DCE-MRI and plaque burden by MRI. On the same platform, Senders et al.<sup>29</sup> have recently employed combined PET/MR for in-depth atherosclerotic plaque phenotyping encompassing the quantification of inflammation by <sup>18</sup>F-FDG PET, microcalcification (a parameter related to inflammation) by <sup>18</sup>F sodium fluoride (NaF) PET, plaque burden by 3D MRI and plaque permeability/neovascularization by 3D DCE-MRI (Figure 1). Additionally, the authors used non-invasive PET/MRI to screen 3 novel nanobody-based PET tracers directed, respectively, against vascular cell adhesion molecule (VCAM)-1, lectin-like oxidized low-density lipoprotein receptor (LOX)-1, and macrophage mannose receptor (MMR). After thorough evaluation of the <sup>64</sup>Cu-labeled nanobodies in mice and rabbits (Figure 1A), the MMR specific nanobody was selected for labeling with the more clinically relevant isotope <sup>68</sup>Ga and applied for plaque characterization in atherosclerotic rabbits by PET/MRI (Figure 1B). An increase in all imaging metrics was observed during plaque progression, in concordance with histological measurements (Figure 1B). Similarly, other studies have also employed combined PET/MR to evaluate novel PET atherosclerosis tracers in rabbits, such as <sup>18</sup>F-labeled modified polyglucose nanoparticles as a macrophage burden marker<sup>30</sup>, <sup>64</sup>Cu-labeled diacetyl-bis(N-methylthiosemicarbazone) (ATSM) as a marker of hypoxia<sup>31</sup>, <sup>89</sup>Zr-labeled antigen-binding fragments against oxidation epitopes (Fab LA25)<sup>32</sup>, or <sup>89</sup>Zr-labeled hyaluronan nanoparticles<sup>33</sup>. Finally, Ludvigsen et al.<sup>34</sup> have also applied combined <sup>18</sup>F-FDG PET/MRI to evaluate plaque phenotype in Gottingen minipigs. Notably, the authors found a good correlation between <sup>18</sup>F-FDG plaque uptake by PET/MRI and expression of genes involved in plaque inflammation, with marked differences between atherosclerotic and control pigs, and pigs removed from high fat diet. These results support the potential of both this imaging technique and the animal model for translational imaging studies in atherosclerosis.

## PET/MRI of the heart and brain after ischemia

Combined PET/MRI is also increasingly being used in clinical and pre-clinical studies to gain insight into the pathophysiology of the heart and brain after ischemia. In early studies, Lee et al.<sup>35</sup> used sequential PET and MRI to improve the assessment of myocardial infarction in mice (Figure 2A). Since PET and MRI were acquired on different machines, the authors designed a custom-made mouse bed and a PET/CT gantry adapter allowing to seamlessly transfer the mouse between the two scanners. In addition, a custom-built ‘vest’ consisting of several loops of PE50 tubing filled with 15% iodine water (visible by both CT and MRI) was placed around the mouse chest. A two-step approach was taken to co-register PET and MR images, by initially obtaining rough alignment of the two datasets using the holder position, followed by translational and rotational alignment using a cross correlation algorithm. Testing of a <sup>18</sup>F phantom revealed a peak correlation of 0.91 +/- 0.02 between MRI and PET signal, implying excellent co-registration. This sophisticated setup allowed accurately matching infarct scar areas delineated by late gadolinium enhancement (LGE) MRI with infarct inflammation by <sup>18</sup>F-FDG PET, and provided significantly valuable insights on the time course of <sup>18</sup>F-FDG activity and myeloid cell recruitment into the infarcted and remote myocardium during the time course of the experiment. Using the same co-registration approach, Vandoorne et al.<sup>36</sup> used sequential PET/CT and MR imaging with <sup>68</sup>Ga-NODAGA-RGD, an integrin  $\alpha v \beta 3$ -specific PET tracer, and RhoB-albumin-Gd-DTPA to demonstrate, respectively, increased endothelial cell activation and permeability in the bone marrow of mice injected with the Toll-like receptor (TLR) ligand lipopolysaccharide. While this study is not strictly specific to atherosclerosis, it shows how sequential PET/MRI may be useful to probe vascular remodeling in hematopoietic organs following emergency hematopoiesis, which also occurs after cardiovascular events. Taking this a step forward, Buscher et al.<sup>37</sup> used a prototype small animal PET/MRI system consisting of a 7T small-animal MRI scanner (ClinScan; Bruker BioSpin MRI) equipped with a custom-designed PET insert, to simultaneously evaluate cardiac metabolism and function in mice after myocardial infarction. PET images acquired on this prototype system were compared to a high-resolution standalone PET scanner. While demonstrating significantly lower count sensitivity, left ventricular function evaluated using the PET insert was in good agreement between the two scanners and with MRI. Furthermore, while infarct to remote myocardium contrast was lower in images acquired with the PET insert, this setup still allowed for the accurate detection of cardiac inflammation after ischemia.

In the brain, only a handful of clinical<sup>38</sup> and pre-clinical studies so far have employed simultaneous PET/MRI to gain insights into the pathophysiology of stroke. In mice, Ouyang et al.<sup>39</sup> described the utilization of a standalone integrated PET and MRI system to simultaneously monitor drops in water diffusion and glucose utilization using diffusion weighted imaging (DWI) and <sup>18</sup>F-FDG PET in the brain of mice subjected to cerebral hypoxia-ischemia. Rather than applying these techniques at a specific time point after induction of ischemia, integrated PET/MRI allowed follow-up of dynamic changes in both these parameters during the hypoxic stimulus using multi-parametric, multi-modal imaging. Werner et al.<sup>40</sup> instead employed a clinical PET/MRI system to evaluate the concordance between perfusion-weighted MRI and [<sup>15</sup>O]H<sub>2</sub>O PET in 10 human subjects and 3 male

merino sheep after ischemic stroke (Figure 2B), with the aim of improving the selection of patients who may benefit from thrombolysis. This work demonstrated feasibility of combined PET/MRI in this patient population, with no impact on standard clinical workflow. Only moderate agreement was found between perfusion weighted MRI and [ $^{15}\text{O}$ ]H $_2\text{O}$  PET, with correlations being higher for sheep than in humans, most likely because of a more homogeneous disease etiology in the animal model.

## Whole-body PET/MRI: a tool in the development of novel nanotherapies

In addition to the therapeutic studies mentioned in previous sections, combined PET/MRI can aid in the development and validation of novel anti-atherosclerosis nanotherapies, beyond the assessment of therapeutic efficacy in the vasculature alone. While extensive and sophisticated *ex vivo* assays are typically employed to study therapeutic effects in mice, in large animal models *in vivo* translational PET/MRI can be used to assess a nanoformulation's pharmacokinetics, biodistribution and plaque targeting (through  $^{89}\text{Zr}$  radiolabeling) as well as therapeutic efficacy. For example, as a follow up to several studies already demonstrating plaque accumulation of long circulating nanoparticles in atherosclerotic rabbits<sup>26, 41–43</sup> and patients<sup>44</sup>, a recent study by Lobatto et al.<sup>45</sup> employed longitudinal imaging with both PET/CT and PET/MRI to evaluate the distribution and plaque targeting of  $^{89}\text{Zr}$ -labeled liposomal nanoparticles in a rabbit model of atherosclerosis. Aortic uptake of  $^{89}\text{Zr}$ -labeled liposomes by PET/CT and PET/MRI was highly correlated. However, better than PET/CT, integrated PET/MRI allowed co-localizing nanoparticle uptake with areas of increased plaque permeability/neovascularization by 3D DCE-MRI. Another study<sup>46</sup> also used serial PET/MRI to investigate the organ distribution of reconstituted high-density lipoprotein (HDL) in the rabbit model. While HDL is an important class of lipoproteins involved in reverse cholesterol transport from atherosclerotic plaques, thanks to their affinity for plaque macrophages they have also been proposed as a potential plaque macrophage mapping agent<sup>47, 48</sup>. In this study, two radiolabeling strategies were pursued, with  $^{89}\text{Zr}$  attached to either APOA1 ( $^{89}\text{Zr}$ -AI-HDL) or a phospholipid ( $^{89}\text{Zr}$ -PL-HDL) through the chelator deferoxamine B (DFO), which allowed studying the kinetics of HDL's main components by PET/MRI. Rabbits were imaged at several time points after nanoparticle injection (1 hour, 1, 2, 3 and 5 days). While early imaging time points showed that both  $^{89}\text{Zr}$ -AI-HDL and  $^{89}\text{Zr}$ -PL-HDL mainly resided in the blood pool, later time points showed accumulation in kidneys, liver and spleen. Both particles also accumulated in the bone, and specifically in the bone marrow, as confirmed by *ex vivo* analysis. Higher aortic accumulation of both  $^{89}\text{Zr}$ -AI-HDL and  $^{89}\text{Zr}$ -PL-HDL in atherosclerotic versus control animals was found at 5 days post injection, while the quantification of aortic signal at earlier time points was confounded by residual blood pool activity. Regardless of the radiolabel location, both particles were found to target plaque macrophages and monocytes.

Following extensive mouse work<sup>47, 48</sup>, two recent studies have used whole-body PET/MRI in large animals in an effort to assess the translational potential of nanoimmunotherapeutics for atherosclerosis. Binderup et al.<sup>49</sup> investigated the *in vivo* behavior and therapeutic efficacy of HDL loaded with simvastatin (S-HDL) by multimodal clinical imaging in rabbit and pig models of atherosclerosis (Figure 3). Ensuing PET/CT biodistribution imaging of  $^{89}\text{Zr}$ -labeled S-HDL ( $^{89}\text{Zr}$ -[S]-HDL), vessel wall targeting was evaluated in the rabbit

abdominal aorta and in the pigs' femoral arteries. Both *in vivo* PET/MRI and *ex vivo* assays indicated that while  $^{89}\text{Zr}$ -[S]-HDL accumulated preferentially in atherosclerotic plaques, its accumulation was not merely governed by increased permeability, but by active targeting of plaque macrophages. Advanced plaque phenotyping by a workflow integrating  $^{18}\text{F}$ -fluorothymidine ( $^{18}\text{F}$ -FLT) PET,  $^{18}\text{F}$ -FDG PET, 3D DCE-MRI and high-resolution T2-weighted MRI allowed studying, respectively, macrophage proliferation, inflammation, vessel wall permeability and plaque burden. This protocol was applied to assess S-HDL's therapeutic efficacy and revealed decreased plaque burden (vessel wall area) in treated atherosclerotic rabbits, and halted plaque progression in pigs, compared to untreated animals. In a separate study by the same research group, Lameijer et al.<sup>50</sup> have used integrated PET/MRI of non-human primates to investigate the safety and biodistribution of a novel nanoimmunotherapy aimed at hampering CD40 - CD40 ligand co-stimulation through tumor necrosis factor receptor-associated factor 6 (TRAF6) inhibition. The authors developed a fully integrated protocol based on high-resolution, whole-body 3 dimensional MRI and dynamic PET to track organ accumulation of  $^{89}\text{Zr}$ -labeled TRAF6i-HDL dynamically and longitudinally in this model on a whole body level. Non-human primates were imaged using dynamic PET for the first hour after tracer administration, and then longitudinally at 1, 2 and 3 days after injection using static PET imaging. Initially, strong uptake in the kidneys was observed, followed by uptake in the spleen and liver, which persisted at later time-points. Importantly, PET/MRI findings were confirmed by *ex vivo* radiometric assays performed at the 72 hours time point, thereby suggesting that whole body PET/MRI is a viable strategy to quantify biodistribution of novel nanoimmunotherapeutics *in vivo*, non-invasively and longitudinally.

## The future of pre-clinical cardiovascular PET/MRI: challenges and new opportunities

As it emerges from the sections above, while the use of cardiovascular PET/MRI in pre-clinical models is still in its infancy, the application of this technology holds great promise to improve our understanding of atherogenesis and the assessment of novel anti-atherosclerotic strategies. However, there are still remaining challenges in the application of combined PET/MRI to pre-clinical atherosclerosis research, mostly related to the limited availability of commercial PET/MR scanners for small animal imaging, and to difficulties in performing accurate PET attenuation correction for large animal models on clinical PET/MR imagers.

While commercial PET/MR small animal imagers are available, they are offered by most vendors as a combination of pre-clinical PET systems with 1 or 3 tesla (T) MRI systems. These field strengths are quite low compared to most standalone small animal MR scanners and might not be suitable for high-resolution imaging of the atherosclerotic arterial wall in small rodents. Other solutions, consisting of either sequential systems or PET inserts have been tested at higher field strengths, up to 9.4T, which are better suited for vascular imaging. However, sequential systems do not offer the significant advantage of simultaneous PET and MR acquisitions, such as monitoring different biological processes at the same time. On the other hand, while often offering the flexibility of being also used as standalone PET systems,



PET inserts might require additional maintenance and pose significant hurdles during their use.

The use of clinical PET/MR scanners for clinical and large animal pre-clinical cardiovascular research also faces specific challenges. While correlation between tracer uptake values between PET/CT and PET/MRI has been found to be strong<sup>46</sup>, several studies have reported a significant bias and underestimation of PET standardized uptake value (SUV), a validated measure of tracer uptake, by PET/MRI compared to PET/CT<sup>51</sup>. In these studies, the main cause of SUV underestimation was believed to be related to issues specific to PET/MRI attenuation correction, such as assignment of wrong attenuation values due to incorrect segmentation and classification of MR images acquired for the purposes of attenuation correction<sup>52</sup>, or the lack of a bone compartment in many MR-based attenuation maps<sup>53, 54</sup>. In the case of cardiovascular imaging, this may result in significant errors in the quantification of PET tracer uptake in vascular structures close to bone, such as the carotid artery, and abdominal aorta (close to the spine), or for evaluation of the bone marrow itself. Several approaches, such as ultra-short or zero echo time (TE) imaging or 'atlas'-based attenuation maps<sup>55</sup>, have been proposed to overcome this issue. However, these solutions may add a layer of complexity to the evaluation of PET/MRI data, as they require *ad hoc* post-processing, or, such as in the case of atlases, they may be mainly built for human applications and are therefore not suitable for pre-clinical imaging. In this landscape, MR-based attenuation correction of PET data in pre-clinical imaging remains a challenge, especially for large animal models of disease, and may still require significant efforts to process PET image reconstruction offline, on a case by case basis.

Despite these lingering challenges, there are also several areas where the application of combined PET/MRI may greatly benefit pre-clinical cardiovascular imaging in the near future. As demonstrated by several pre-clinical and clinical atherosclerosis studies, PET/MRI offers the distinct benefit of allowing co-localization of the PET signal with different plaque features (such as wall thickness, or composition) evaluated by multi-parametric MRI, employing either different MR weightings, or readouts (such as perfusion imaging). As already described, this unique approach allows the combination of different multi-modality imaging features for in-depth plaque phenotyping. Furthermore, the high resolution and superior soft tissue contrast of MR images, allow the application of partial volume error (PVE) correction techniques to PET images, to improve the definition of vascular PET tracer uptake. Partial volume errors consist in the contamination of signal from neighboring image voxels, leading to inaccurate quantification. These artifacts are particularly relevant to vascular imaging, either clinical or pre-clinical, due to the intrinsically small size of the arterial vessel wall. Several clinical studies have employed high-resolution vascular MR data to improve the resolution of PET images<sup>56, 57</sup>, and therefore the quantification of vascular radiotracer uptake. In small animals, PVE correction techniques have been used, for example, to improve the image-derived quantification of blood tracer activity (the so-called arterial input function, AIF) in the rabbit abdominal aorta<sup>58</sup>, and in the mouse left ventricle<sup>59</sup>, to aid dynamic imaging studies.

Combined PET/MRI may also prove fundamental in improving quality and contrast of PET images of the moving heart<sup>3</sup>, for the more accurate assessment of vascular inflammation or

myocardial viability after ischemia, or for assessment of the coronary arteries<sup>60</sup>. Different than PET/CT, where cardiac and respiratory motion are typically dealt with by ‘gating’ acquired PET data on the basis of external ECG monitors and respiratory bellows, integrated PET/MRI allows for motion correction of the PET data using the dynamic acquisition of MR images with high spatiotemporal resolution during the cardiac and respiratory cycles. From these MR images, motion vector fields can be calculated and applied to the whole set of PET emission data, to reconstruct high signal-to-noise, motion-corrected PET images. Furthermore, this approach allows estimating attenuation maps during the cardiac and respiratory cycles, thereby eliminating possible image artifacts due to motion in the attenuation maps themselves. While several clinical cardiovascular PET/MRI studies have addressed this topic<sup>61</sup>, some groups have also tested this framework in pre-clinical models. For example, in rabbits and non-human primates, Ouyang et al.<sup>62</sup> have shown the development of a procedure to dynamically acquire information on cardiac and respiratory motion by MRI and applied derived motion vector fields to simultaneously acquired PET images, for the purpose of motion correction. The authors showed that MR-based motion correction improved detection of hot spheres implanted in the rabbits’ diaphragm and liver, without increasing image noise with respect to a six times longer gated acquisition. Similar results were found in the non-human primate experiment.

Finally, PET/MRI might be instrumental to the development of ‘smart’, bimodal imaging probes for better characterization of pathophysiological processes in the vasculature or other organs involved in cardiovascular disease. As an example, Frullano et al.<sup>63</sup> have described the use of combined PET/MRI to accurately measure pH with the pH-sensitive agent GdDOTA-4AMP. Since the relaxivity of GdDOTA-4AMP is pH dependent, the concentration of the agent, which is needed for absolute pH quantification, cannot be extrapolated solely from changes in tissue T1 relaxation time. The authors elegantly proposed to radiolabel GdDOTA-4AMP with the radioisotope <sup>18</sup>F to accurately measure the MR contrast agent concentration by simultaneous PET imaging. This bimodal imaging strategy enabled absolute quantification of tissue pH in one imaging session. While this example is not specific to atherosclerosis and cardiovascular disease, one could envision that similar strategies might allow the development of bimodal PET/MR imaging probes that would fully exploit the synergy of these two imaging modalities for a better characterization of pathophysiological processes in the vessel wall and hematopoietic organs.

## Concluding remarks

In this review we have provided an overview of the main applications of pre-clinical PET/MRI in small and large animal models of cardiovascular disease. In the pre-clinical arena, combined PET/MRI offers distinct advantages over PET/CT for in depth phenotyping of atherosclerotic plaques, the heart and brain after ischemia and as a tool to facilitate the development of novel anti-atherosclerosis compounds. Furthermore, whole-body imaging with PET/MRI allows investigating atherosclerosis beyond the vasculature, heart and brain, to include the assessment of hematopoietic organs, implicated in the immune response which lies at the basis of atherogenesis. Despite remaining challenges, we foresee that in the near future the pre-clinical applications of PET/MRI may greatly expand. The combination of *in vivo*, non-invasive, multi-parametric, whole-body PET/MRI together with sophisticated

*ex vivo* immunological assays possible in animal models may prove an invaluable tool to gain further insights into the pathophysiology of atherosclerosis, and will allow to fully exploit the synergistic value of these two complementary imaging modalities.

## Sources of Funding.

This work was supported by American Heart Association 16SDG27250090 (to C.C) and 16SDG31390007 (to C.P.-M.); the National Institutes of Health grants R01 HL125703 and R01 HL118440 (to W.J.M.M.) and R01 HL071021, R01 HL135878, R01 HL143814 (to Z.A.F.).

## Bibliography

1. Calcagno C, Mulder WJ, Nahrendorf M, Fayad ZA. Systems biology and noninvasive imaging of atherosclerosis. *Arterioscler Thromb Vasc Biol.* 2016;36:e1–8 [PubMed: 26819466]
2. Vandoorne K, Nahrendorf M. Multiparametric imaging of organ system interfaces. *Circ Cardiovasc Imaging.* 2017;10
3. Robson PM, Dey D, Newby DE, Berman D, Li D, Fayad ZA, Dweck MR. Mr/pet imaging of the cardiovascular system. *JACC Cardiovasc Imaging.* 2017;10:1165–1179 [PubMed: 28982570]
4. Joseph P, Tawakol A. Imaging atherosclerosis with positron emission tomography. *Eur Heart J.* 2016;37:2974–2980 [PubMed: 27125951]
5. Tawakol A, Migrino RQ, Bashian GG, Bedri S, Vermylen D, Cury RC, Yates D, LaMuraglia GM, Furie K, Houser S, Gewirtz H, Muller JE, Brady TJ, Fischman AJ. In vivo 18f-fluorodeoxyglucose positron emission tomography imaging provides a noninvasive measure of carotid plaque inflammation in patients. *J Am Coll Cardiol.* 2006;48:1818–1824 [PubMed: 17084256]
6. Vucic E, Dickson SD, Calcagno C, Rudd JH, Moshier E, Hayashi K, Mounessa JS, Roytman M, Moon MJ, Lin J, Tsimikas S, Fisher EA, Nicolay K, Fuster V, Fayad ZA. Pioglitazone modulates vascular inflammation in atherosclerotic rabbits noninvasive assessment with fdg-pet-ct and dynamic contrast-enhanced mr imaging. *JACC Cardiovasc Imaging.* 2011;4:1100–1109 [PubMed: 21999870]
7. Vucic E, Calcagno C, Dickson SD, Rudd JH, Hayashi K, Bucierius J, Moshier E, Mounessa JS, Roytman M, Moon MJ, Lin J, Ramachandran S, Tanimoto T, Brown K, Kotsuma M, Tsimikas S, Fisher EA, Nicolay K, Fuster V, Fayad ZA. Regression of inflammation in atherosclerosis by the Ixr agonist r211945: A noninvasive assessment and comparison with atorvastatin. *JACC Cardiovasc Imaging.* 2012;5:819–828 [PubMed: 22897996]
8. Beitzke D, Rasul S, Lassen ML, Pichler V, Senn D, Stelzmuller ME, Nolz R, Loewe C, Hacker M. Assessment of myocardial viability in ischemic heart disease by pet/mri: Comparison of left ventricular perfusion, hibernation, and scar burden. *Acad Radiol.* 2019
9. Kunze KP, Dirschinger RJ, Kossmann H, Hanus F, Ibrahim T, Laugwitz KL, Schwaiger M, Rischpler C, Nekolla SG. Quantitative cardiovascular magnetic resonance: Extracellular volume, native t1 and 18f-fdg pet/cmr imaging in patients after revascularized myocardial infarction and association with markers of myocardial damage and systemic inflammation. *J Cardiovasc Magn Reson.* 2018;20:33 [PubMed: 29792210]
10. Dutta P, Courties G, Wei Y, Leuschner F, Gorbato R, Robbins CS, Iwamoto Y, Thompson B, Carlson AL, Heidt T, Majmudar MD, Lasitschka F, Eitzrodt M, Waterman P, Waring MT, Chicoine AT, van der Laan AM, Niessen HW, Piek JJ, Rubin BB, Butany J, Stone JR, Katus HA, Murphy SA, Morrow DA, Sabatine MS, Vinegoni C, Moskowitz MA, Pittet MJ, Libby P, Lin CP, Swirski FK, Weissleder R, Nahrendorf M. Myocardial infarction accelerates atherosclerosis. *Nature.* 2012;487:325–329 [PubMed: 22763456]
11. Emami H, Singh P, MacNabb M, Vucic E, Lavender Z, Rudd JH, Fayad ZA, Lehrer-Graiwer J, Korsgren M, Figueroa AL, Fredrickson J, Rubin B, Hoffmann U, Truong QA, Min JK, Baruch A, Nasir K, Nahrendorf M, Tawakol A. Splenic metabolic activity predicts risk of future cardiovascular events: Demonstration of a cardioplenic axis in humans. *JACC Cardiovasc Imaging.* 2015;8:121–130 [PubMed: 25577441]

12. Joshi NV, Toor I, Shah AS, Carruthers K, Vesey AT, Alam SR, Sills A, Hoo TY, Melville AJ, Langlands SP, Jenkins WS, Uren NG, Mills NL, Fletcher AM, van Beek EJ, Rudd JH, Fox KA, Dweck MR, Newby DE. Systemic atherosclerotic inflammation following acute myocardial infarction: Myocardial infarction begets myocardial infarction. *J Am Heart Assoc.* 2015;4:e001956 [PubMed: 26316523]
13. Pirro M, Simental-Mendia LE, Bianconi V, Watts GF, Banach M, Sahebkar A. Effect of statin therapy on arterial wall inflammation based on 18f-fdg pet/ct: A systematic review and meta-analysis of interventional studies. *J Clin Med.* 2019;8
14. Tarkin JM, Joshi FR, Rudd JH. Pet imaging of inflammation in atherosclerosis. *Nat Rev Cardiol.* 2014;11:443–457 [PubMed: 24913061]
15. Kerwin WS, Miller Z, Yuan C. Imaging of the high-risk carotid plaque: Magnetic resonance imaging. *Semin Vasc Surg.* 2017;30:54–61 [PubMed: 28818259]
16. Coolen BF, Calcagno C, van Ooij P, Fayad ZA, Strijkers GJ, Nederveen AJ. Vessel wall characterization using quantitative mri: What's in a number? *MAGMA.* 2018;31:201–222 [PubMed: 28808823]
17. Phinikaridou A, Andia ME, Lacerda S, Lorrio S, Makowski MR, Botnar RM. Molecular mri of atherosclerosis. *Molecules.* 2013;18:14042–14069 [PubMed: 24232739]
18. Wang J, Yarnykh VL, Yuan C. Enhanced image quality in black-blood mri using the improved motion-sensitized driven-equilibrium (imsde) sequence. *J Magn Reson Imaging.* 2010;31:1256–1263 [PubMed: 20432365]
19. Mihai G, Winner MW, Raman SV, Rajagopalan S, Simonetti OP, Chung YC. Assessment of carotid stenosis using three-dimensional t2-weighted dark blood imaging: Initial experience. *J Magn Reson Imaging.* 2012;35:449–455 [PubMed: 22147541]
20. Balu N, Zhou Z, Hippe DS, Hatsukami T, Mossa-Basha M, Yuan C. Accelerated multi-contrast high isotropic resolution 3d intracranial vessel wall mri using a tailored k-space undersampling and partially parallel reconstruction strategy. *MAGMA.* 2019;32:343–357 [PubMed: 30607664]
21. LaForest R, Woodard PK, Gropler RJ. Cardiovascular pet/mri: Challenges and opportunities. *Cardiol Clin.* 2016;34:25–35 [PubMed: 26590777]
22. Bigalke B, Phinikaridou A, Andia ME, Cooper MS, Schuster A, Wurster T, Onthank D, Munch G, Blower P, Gawaz M, Nagel E, Botnar RM. Pet/ct and mr imaging biomarker of lipid-rich plaques using [64cu]-labeled scavenger receptor (cd68-fc). *Int J Cardiol.* 2014;177:287–291 [PubMed: 25499394]
23. Li X, Bauer W, Israel I, Kreissl MC, Weirather J, Richter D, Bauer E, Herold V, Jakob P, Buck A, Frantz S, Samnick S. Targeting p-selectin by gallium-68-labeled fucoidan positron emission tomography for noninvasive characterization of vulnerable plaques: Correlation with in vivo 17.6t mri. *Arterioscler Thromb Vasc Biol.* 2014;34:1661–1667 [PubMed: 24903095]
24. Jarrett BR, Correa C, Ma KL, Louie AY. In vivo mapping of vascular inflammation using multimodal imaging. *PLoS One.* 2010;5:e13254 [PubMed: 20949008]
25. Pellico J, Llop J, Fernandez-Barahona I, Bhavesh R, Ruiz-Cabello J, Herranz F. Iron oxide nanoradiomaterials: Combining nanoscale properties with radioisotopes for enhanced molecular imaging. *Contrast Media Mol Imaging.* 2017;2017:1549580 [PubMed: 29358900]
26. Lobatto ME, Calcagno C, Metselaar JM, Storm G, Stroes ES, Fayad ZA, Mulder WJ. Imaging the efficacy of anti-inflammatory liposomes in a rabbit model of atherosclerosis by non-invasive imaging. *Methods Enzymol.* 2012;508:211–228 [PubMed: 22449928]
27. Millon A, Dickson SD, Klink A, Izquierdo-Garcia D, Bini J, Lancelot E, Ballet S, Robert P, Mateo de Castro J, Corot C, Fayad ZA. Monitoring plaque inflammation in atherosclerotic rabbits with an iron oxide (p904) and (18)f-fdg using a combined pet/mr scanner. *Atherosclerosis.* 2013;228:339–345 [PubMed: 23582588]
28. Calcagno C, Lairez O, Hawkins J, Kerr SW, Dugas MS, Simpson T, Epskamp J, Robson PM, Eldib M, Bander I, P KR, Ramachandran S, Pruzan A, Kaufman A, Mani V, Ehlgen A, Niessen HG, Broadwater J, Fayad ZA. Combined pet/dce-mri in a rabbit model of atherosclerosis: Integrated quantification of plaque inflammation, permeability, and burden during treatment with a leukotriene a4 hydrolase inhibitor. *JACC Cardiovasc Imaging.* 2018;11:291–301 [PubMed: 29413439]

29. Senders ML, Hernot S, Carlucci G, van de Voort JC, Fay F, Calcagno C, Tang J, Alaarg A, Zhao Y, Ishino S, Palmisano A, Boeykens G, Meerwaldt AE, Sanchez-Gaytan BL, Baxter S, Zendman L, Lobatto ME, Karakatsanis NA, Robson PM, Broisat A, Raes G, Lewis JS, Tsimikas S, Reiner T, Fayad ZA, Devoogdt N, Mulder WJM, Perez-Medina C. Nanobody-facilitated multiparametric pet/mri phenotyping of atherosclerosis. *JACC Cardiovasc Imaging*. 2018
30. Kelihier EJ, Ye YX, Wojtkiewicz GR, Aguirre AD, Tricot B, Senders ML, Groenen H, Fay F, Perez-Medina C, Calcagno C, Carlucci G, Reiner T, Sun Y, Courties G, Iwamoto Y, Kim HY, Wang C, Chen JW, Swirski FK, Wey HY, Hooker J, Fayad ZA, Mulder WJ, Weissleder R, Nahrendorf M. Polyglucose nanoparticles with renal elimination and macrophage avidity facilitate pet imaging in ischaemic heart disease. *Nat Commun*. 2017;8:14064 [PubMed: 28091604]
31. Nie X, Laforest R, Elvington A, Randolph GJ, Zheng J, Voller T, Abendschein DR, Lapi SE, Woodard PK. Pet/mri of hypoxic atherosclerosis using 64cu-atm in a rabbit model. *J Nucl Med*. 2016;57:2006–2011 [PubMed: 27390157]
32. Senders ML, Que X, Cho YS, Yeang C, Groenen H, Fay F, Calcagno C, Meerwaldt AE, Green S, Miu P, Lobatto ME, Reiner T, Fayad ZA, Witztum JL, Mulder WJM, Perez-Medina C, Tsimikas S. Pet/mr imaging of malondialdehyde-acetaldehyde epitopes with a human antibody detects clinically relevant atherothrombosis. *J Am Coll Cardiol*. 2018;71:321–335 [PubMed: 29348025]
33. Beldman TJ, Senders ML, Alaarg A, Perez-Medina C, Tang J, Zhao Y, Fay F, Deichmoller J, Born B, Desclos E, van der Wel NN, Hoebe RA, Kohen F, Kartvelishvily E, Neeman M, Reiner T, Calcagno C, Fayad ZA, de Winther MPJ, Lutgens E, Mulder WJM, Kluza E. Hyaluronan nanoparticles selectively target plaque-associated macrophages and improve plaque stability in atherosclerosis. *ACS Nano*. 2017;11:5785–5799 [PubMed: 28463501]
34. Ludvigsen TP, Pedersen SF, Vegge A, Ripa RS, Johannesen HH, Hansen AE, Lofgren J, Schumacher-Petersen C, Kirk RK, Pedersen HD, Christoffersen BO, Orbaek M, Forman JL, Klausen TL, Olsen LH, Kjaer A. (18)f-fdg pet/mr-imaging in a gottingen minipig model of atherosclerosis: Correlations with histology and quantitative gene expression. *Atherosclerosis*. 2019;285:55–63 [PubMed: 31004968]
35. Lee WW, Marinelli B, van der Laan AM, Sena BF, Gorbatov R, Leuschner F, Dutta P, Iwamoto Y, Ueno T, Begieneman MP, Niessen HW, Piek JJ, Vinegoni C, Pittet MJ, Swirski FK, Tawakol A, Di Carli M, Weissleder R, Nahrendorf M. Pet/mri of inflammation in myocardial infarction. *J Am Coll Cardiol*. 2012;59:153–163 [PubMed: 22222080]
36. Vandoorne K, Rohde D, Kim HY, Courties G, Wojtkiewicz G, Honold L, Hoyer FF, Frodermann V, Nayar R, Herisson F, Jung Y, Desogere PA, Vinegoni C, Caravan P, Weissleder R, Sosnovik DE, Lin CP, Swirski FK, Nahrendorf M. Imaging the vascular bone marrow niche during inflammatory stress. *Circ Res*. 2018;123:415–427 [PubMed: 29980569]
37. Buscher K, Judenhofer MS, Kuhlmann MT, Hermann S, Wehrl HF, Schafers KP, Schafers M, Pichler BJ, Stegger L. Isochronous assessment of cardiac metabolism and function in mice using hybrid pet/mri. *J Nucl Med*. 2010;51:1277–1284 [PubMed: 20660390]
38. Werner P, Saur D, Mildner T, Moller H, Classen J, Sabri O, Hoffmann KT, Barthel H. Combined pet/mri: Multimodality insights into acute stroke hemodynamics. *Neurology*. 2016;86:1926–1927 [PubMed: 27185897]
39. Ouyang Y, Judenhofer MS, Walton JH, Marik J, Williams SP, Cherry SR. Simultaneous pet/mri imaging during mouse cerebral hypoxia-ischemia. *J Vis Exp*. 2015
40. Werner P, Saur D, Zeisig V, Ettrich B, Patt M, Sattler B, Jochimsen T, Lobsien D, Meyer PM, Bergh FT, Dreyer A, Boltze J, Classen J, Fritzsche D, Hoffmann KT, Sabri O, Barthel H. Simultaneous pet/mri in stroke: A case series. *J Cereb Blood Flow Metab*. 2015;35:1421–1425 [PubMed: 26174332]
41. Kim Y, Lobatto ME, Kawahara T, Lee Chung B, Mieszawska AJ, Sanchez-Gaytan BL, Fay F, Senders ML, Calcagno C, Becraft J, Tun Saung M, Gordon RE, Stroes ES, Ma M, Farokhzad OC, Fayad ZA, Mulder WJ, Langer R. Probing nanoparticle translocation across the permeable endothelium in experimental atherosclerosis. *Proc Natl Acad Sci U S A*. 2014;111:1078–1083 [PubMed: 24395808]
42. Lobatto ME, Calcagno C, Millon A, Senders ML, Fay F, Robson PM, Ramachandran S, Binderup T, Paridaans MP, Sensarn S, Rogalla S, Gordon RE, Cardoso L, Storm G, Metselaar JM, Contag CH, Stroes ES, Fayad ZA, Mulder WJ. Atherosclerotic plaque targeting mechanism of long-

- circulating nanoparticles established by multimodal imaging. *ACS Nano*. 2015;9:1837–1847 [PubMed: 25619964]
43. Lobatto ME, Calcagno C, Otten MJ, Millon A, Ramachandran S, Paridaans MP, van der Valk FM, Storm G, Stroes ES, Fayad ZA, Mulder WJ, Metselaar JM. Pharmaceutical development and preclinical evaluation of a gmp-grade anti-inflammatory nanotherapy. *Nanomedicine*. 2015;11:1133–1140 [PubMed: 25791805]
44. van der Valk FM, van Wijk DF, Lobatto ME, Verberne HJ, Storm G, Willems MC, Legemate DA, Nederveen AJ, Calcagno C, Mani V, Ramachandran S, Paridaans MP, Otten MJ, Dallinga-Thie GM, Fayad ZA, Nieuwdorp M, Schulte DM, Metselaar JM, Mulder WJ, Stroes ES. Prednisolone-containing liposomes accumulate in human atherosclerotic macrophages upon intravenous administration. *Nanomedicine*. 2015;11:1039–1046 [PubMed: 25791806]
45. Lobatto ME, Binderup T, Robson PM, Giesen LFP, Calcagno C, Witjes J, Fay F, Baxter S, Wessel CH, Eldib M, Bini J, Carlin SD, Stroes ESG, Storm G, Kjaer A, Lewis JS, Reiner T, Fayad ZA, Mulder WJM, Perez-Medina C. Multimodal positron emission tomography imaging to quantify uptake of 89zr-labeled liposomes in the atherosclerotic vessel wall. *Bioconjug Chem*. 2019
46. Perez-Medina C, Binderup T, Lobatto ME, Tang J, Calcagno C, Giesen L, Wessel CH, Witjes J, Ishino S, Baxter S, Zhao Y, Ramachandran S, Eldib M, Sanchez-Gaytan BL, Robson PM, Bini J, Granada JF, Fish KM, Stroes ES, Duivenvoorden R, Tsimikas S, Lewis JS, Reiner T, Fuster V, Kjaer A, Fisher EA, Fayad ZA, Mulder WJ. In vivo pet imaging of hdl in multiple atherosclerosis models. *JACC Cardiovasc Imaging*. 2016;9:950–961 [PubMed: 27236528]
47. Duivenvoorden R, Tang J, Cormode DP, Mieszawska AJ, Izquierdo-Garcia D, Ozcan C, Otten MJ, Zaidi N, Lobatto ME, van Rijs SM, Priem B, Kuan EL, Martel C, Hewing B, Sager H, Nahrendorf M, Randolph GJ, Stroes ES, Fuster V, Fisher EA, Fayad ZA, Mulder WJ. A statin-loaded reconstituted high-density lipoprotein nanoparticle inhibits atherosclerotic plaque inflammation. *Nat Commun*. 2014;5:3065 [PubMed: 24445279]
48. Tang J, Lobatto ME, Hassing L, van der Staay S, van Rijs SM, Calcagno C, Braza MS, Baxter S, Fay F, Sanchez-Gaytan BL, Duivenvoorden R, Sager H, Astudillo YM, Leong W, Ramachandran S, Storm G, Perez-Medina C, Reiner T, Cormode DP, Strijkers GJ, Stroes ES, Swirski FK, Nahrendorf M, Fisher EA, Fayad ZA, Mulder WJ. Inhibiting macrophage proliferation suppresses atherosclerotic plaque inflammation. *Sci Adv*. 2015;1
49. Binderup T, Duivenvoorden R, Fay F, van Leent MMT, Malkus J, Baxter S, Ishino S, Zhao Y, Sanchez-Gaytan B, Teunissen AJP, Frederico YCA, Tang J, Carlucci G, Lyashchenko S, Calcagno C, Karakatsanis N, Soultanidis G, Senders ML, Robson PM, Mani V, Ramachandran S, Lobatto ME, Hutten BA, Granada JF, Reiner T, Swirski FK, Nahrendorf M, Kjaer A, Fisher EA, Fayad ZA, Perez-Medina C, Mulder WJM. Imaging-assisted nanoimmunotherapy for atherosclerosis in multiple species. *Sci Transl Med*. 2019;11
50. Lameijer M, Binderup T, van Leent MMT, Senders ML, Fay F, Malkus J, Sanchez-Gaytan BL, Teunissen AJP, Karakatsanis N, Robson P, Zhou X, Ye Y, Wojtkiewicz G, Tang J, Seijkens TTP, Kroon J, Stroes ESG, Kjaer A, Ochando J, Reiner T, Perez-Medina C, Calcagno C, Fisher EA, Zhang B, Temel RE, Swirski FK, Nahrendorf M, Fayad ZA, Lutgens E, Mulder WJM, Duivenvoorden R. Efficacy and safety assessment of a traf6-targeted nanoimmunotherapy in atherosclerotic mice and non-human primates. *Nat Biomed Eng*. 2018;2:279–292 [PubMed: 30936448]
51. Li X, Heber D, Rausch I, Beitzke D, Mayerhoefer ME, Rasul S, Kreissl M, Mitthausen M, Wadsak W, Hartenbach M, Haug A, Zhang X, Loewe C, Beyer T, Hacker M. Quantitative assessment of atherosclerotic plaques on (18)f-fdg pet/mri: Comparison with a pet/ct hybrid system. *Eur J Nucl Med Mol Imaging*. 2016;43:1503–1512 [PubMed: 26816195]
52. Ladefoged CN, Hansen AE, Keller SH, Holm S, Law I, Beyer T, Hojgaard L, Kjaer A, Andersen FL. Impact of incorrect tissue classification in dixon-based mr-ac: Fat-water tissue inversion. *EJNMMI Phys*. 2014;1:101 [PubMed: 26501459]
53. Bini J, Izquierdo-Garcia D, Mateo J, Machac J, Narula J, Fuster V, Fayad ZA. Preclinical evaluation of mr attenuation correction versus ct attenuation correction on a sequential whole-body mr/pet scanner. *Invest Radiol*. 2013;48:313–322 [PubMed: 23296082]

54. Bini J, Eldib M, Robson PM, Calcagno C, Fayad ZA. Simultaneous carotid pet/mr: Feasibility and improvement of magnetic resonance-based attenuation correction. *Int J Cardiovasc Imaging*. 2016;32:61–71 [PubMed: 25898892]
55. Chen Y, An H. Attenuation correction of pet/mr imaging. *Magn Reson Imaging Clin N Am*. 2017;25:245–255 [PubMed: 28390526]
56. Bini J, Eldib M, Robson PM, Fayad ZA. Wavelet-based partial volume effect correction for simultaneous mr/pet of the carotid arteries. *EJNMMI Phys*. 2014;1:A71 [PubMed: 26501662]
57. Cal-Gonzalez J, Li X, Heber D, Rausch I, Moore SC, Schafers K, Hacker M, Beyer T. Partial volume correction for improved pet quantification in (18)f-naf imaging of atherosclerotic plaques. *J Nucl Cardiol*. 2018;25:1742–1756 [PubMed: 28176255]
58. Deidda D, Karakatsanis NA, Robson PM, Calcagno C, Senders ML, Mulder WJM, Fayad ZA, Aykroyd RG, Tsoumpas C. Hybrid pet/mr kernelised expectation maximisation reconstruction for improved image-derived estimation of the input function from the aorta of rabbits. *Contrast Media Mol Imaging*. 2019;2019:3438093 [PubMed: 30800014]
59. Evans E, Buonincontri G, Izquierdo D, Methner C, Hawkes RC, Ansorge RE, Kreig T, Carpenter TA, Sawiak SJ. Combining mri with pet for partial volume correction improves image-derived input functions in mice. *EJNMMI Phys*. 2014;1:A84 [PubMed: 26501676]
60. Robson PM, Dweck MR, Trivieri MG, Abgral R, Karakatsanis NA, Contreras J, Gidwani U, Narula JP, Fuster V, Kovacic JC, Fayad ZA. Coronary artery pet/mr imaging: Feasibility, limitations, and solutions. *JACC Cardiovasc Imaging*. 2017;10:1103–1112 [PubMed: 28109921]
61. Robson PM, Trivieri M, Karakatsanis NA, Padilla M, Abgral R, Dweck MR, Kovacic JC, Fayad ZA. Correction of respiratory and cardiac motion in cardiac pet/mr using mr-based motion modeling. *Phys Med Biol*. 2018;63:225011 [PubMed: 30426968]
62. Ouyang J, Li Q, El Fakhri G. Magnetic resonance-based motion correction for positron emission tomography imaging. *Semin Nucl Med*. 2013;43:60–67 [PubMed: 23178089]
63. Frullano L, Catana C, Benner T, Sherry AD, Caravan P. Bimodal mr-pet agent for quantitative ph imaging. *Angew Chem Int Ed Engl*. 2010;49:2382–2384 [PubMed: 20191650]

### Highlights

- Pre-clinical PET/MRI has the potential to aid mechanistic studies to gain new insights on the role of inflammation in cardiovascular disease
- Areas where this technology has been applied successfully are: i) vascular imaging, for advanced atherosclerotic plaque phenotyping and evaluation of novel imaging tracers or therapeutic interventions; ii) assessment of the ischemic heart and brain; and iii) whole-body imaging of the hematopoietic system
- Further technical developments, such as optimization of MR-based attenuation maps, or of motion correction strategies, might increase the impact of cardiovascular PET/MRI in the pre-clinical and clinical arenas



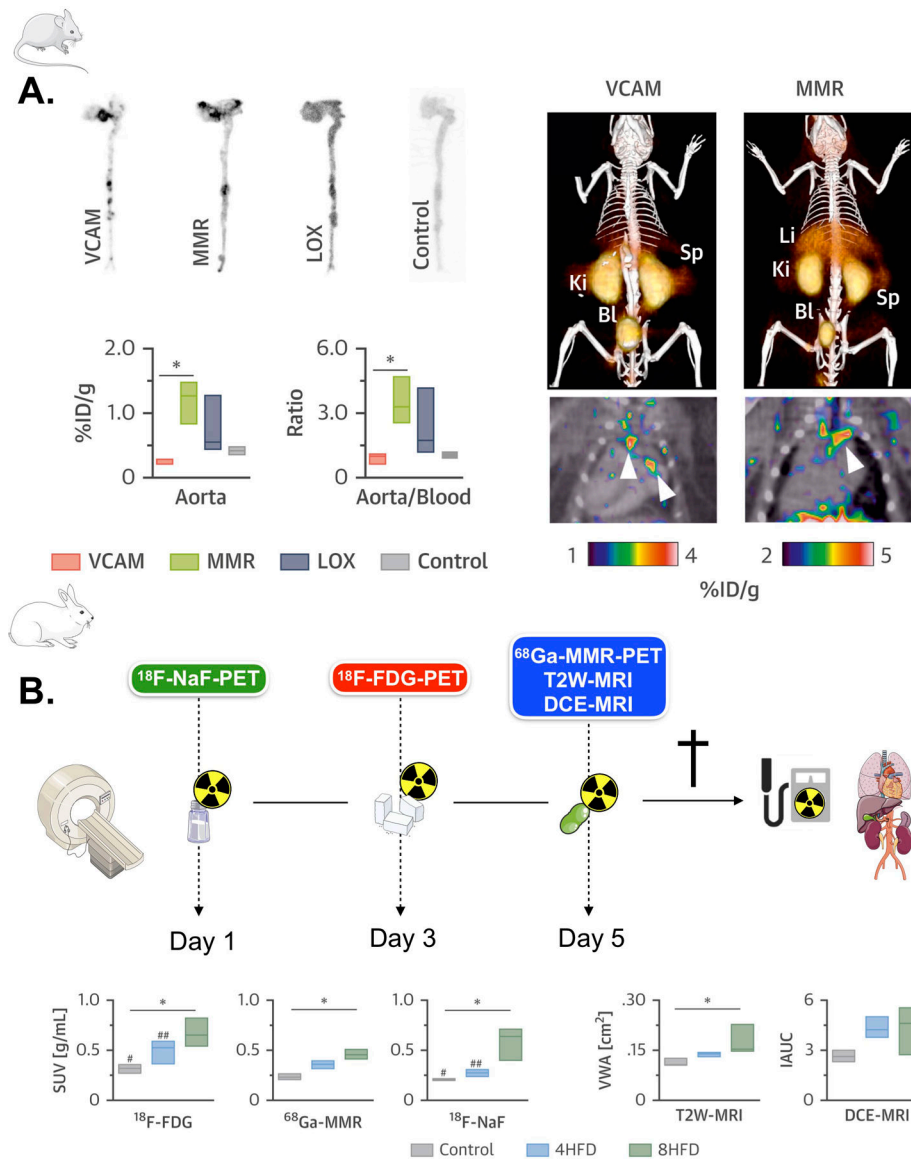


**Figure 1.** (A) **Left**, autoradiography and radioactivity concentration in aortas of *Apoe*<sup>-/-</sup> mice at 3 h post-injection of the corresponding <sup>64</sup>Cu-nanobody (n = 3 per nanobody). **Right**, representative fused PET/CT images 1 h post-injection of <sup>64</sup>Cu-VCAM and <sup>64</sup>Cu-MMR in *Apoe*<sup>-/-</sup> mice. Arrows indicate enhanced uptake at the aortic arch and root, typical sites of atherosclerotic lesions. (B) **Left**, rabbit PET/MR imaging schedule. **Right**, differences in <sup>18</sup>F-FDG (3 h p.i.), <sup>68</sup>Ga-MMR (2 h p.i.), <sup>18</sup>F-NaF (1.5 h p.i.), T2W-MRI and DCE-MRI in healthy and atherosclerotic rabbits (on high-fat diet for 4 months [4HFD] or 8 months [8HFD], n = 3 per group). \*p < 0.05. %ID/g = percentage injected dose per gram of tissue; Bl = bladder; Ki = kidney; Li = liver; Sp = spleen; SUV = standardized uptake value. VCAM, vascular cell adhesion molecule. MMR, macrophage mannose receptor. LOX, lectin-like oxidized low-density lipoprotein receptor. <sup>18</sup>F-NaF PET, <sup>18</sup>F sodium fluoride positron emission tomography. <sup>18</sup>F-FDG PET, <sup>18</sup>F fluorodeoxyglucose positron emission

tomography. T2W-MRI, T2 weighted magnetic resonance imaging. DCE-MRI, dynamic contrast enhanced magnetic resonance imaging. HFD, high fat diet. Adapted from Senders et al<sup>29</sup>.

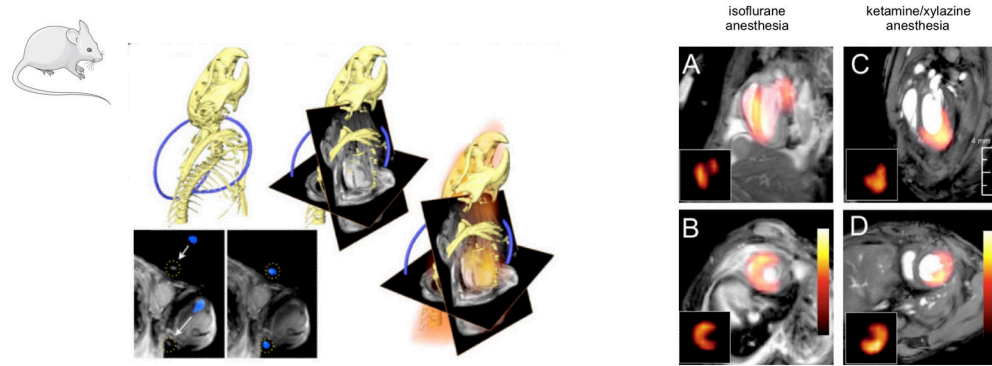
Author Manuscript

Author Manuscript

Author Manuscript

Author Manuscript

### A. Myocardial infarction



### B. Stroke

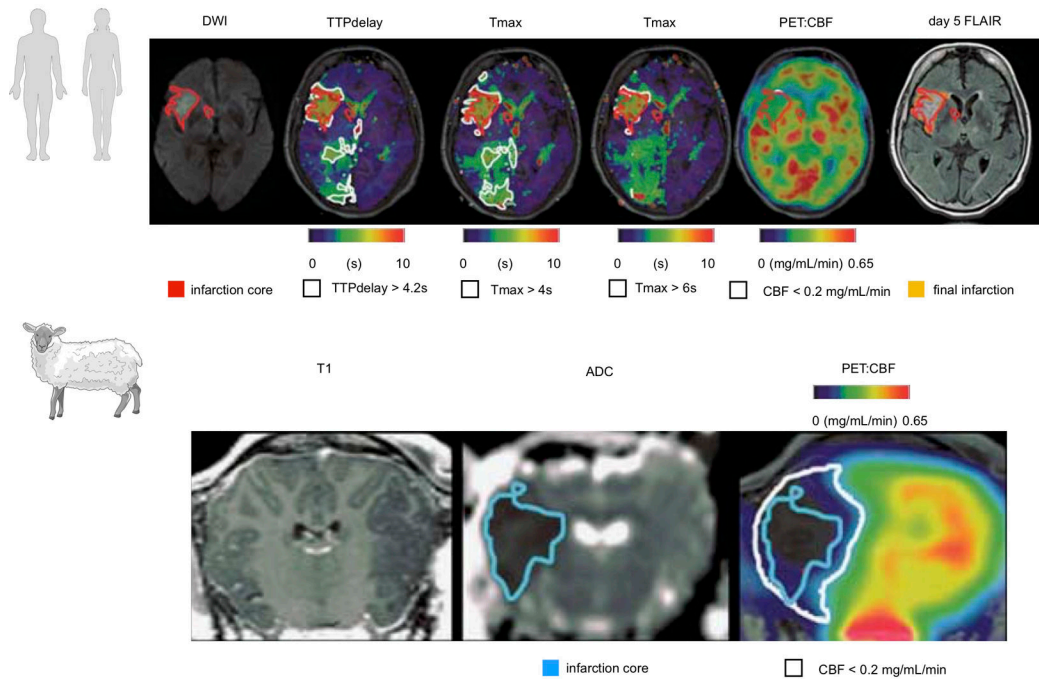


**Figure 2.**

(A) PET/MRI in a mouse with myocardial infarction. PET and MR data was acquired on two separate scanners, and then fused after a process of co-registration aided by a system of fiducial markers. On the left, three-dimensional CT data show the skeleton and a part of the fiducial marker in blue. This allows fusion of CT and MRI matrices, as shown in the center. On the right side, PET data together with angled MR images used during cardiac MRI acquisition are shown. At the far right, fused MR and PET data in a mouse with myocardial infarction are displayed and show different patterns of <sup>18</sup>F-FDG uptake under different anesthesia regimens. Adapted from Lee et al<sup>35</sup> (B) The top row shows [<sup>15</sup>O]H<sub>2</sub>O PET/MRI in a typical human middle cerebral artery (MCA) infarction. Diffusion-weighted MRI shows a disturbance in the right MCA territory (red-bordered area, 22 mL). Perfusion[MRI] flow delays in the right posterior cerebral artery territory did not result in a perfusion restriction according to PET and may thus indicate sufficient collateral flow secondary to the MCA

occlusion. The bottom row, shows [15O]H<sub>2</sub>O PET/MRI 4.5 hours after middle cerebral artery occlusion in sheep. ADC imaging indicated a respective disturbance (blue-bordered area). According to perfusion[<sup>15</sup>O]PET, penumbral volume was 9.8mL (white-bordered area in upper row). Adapted from Werner et al.<sup>40</sup>

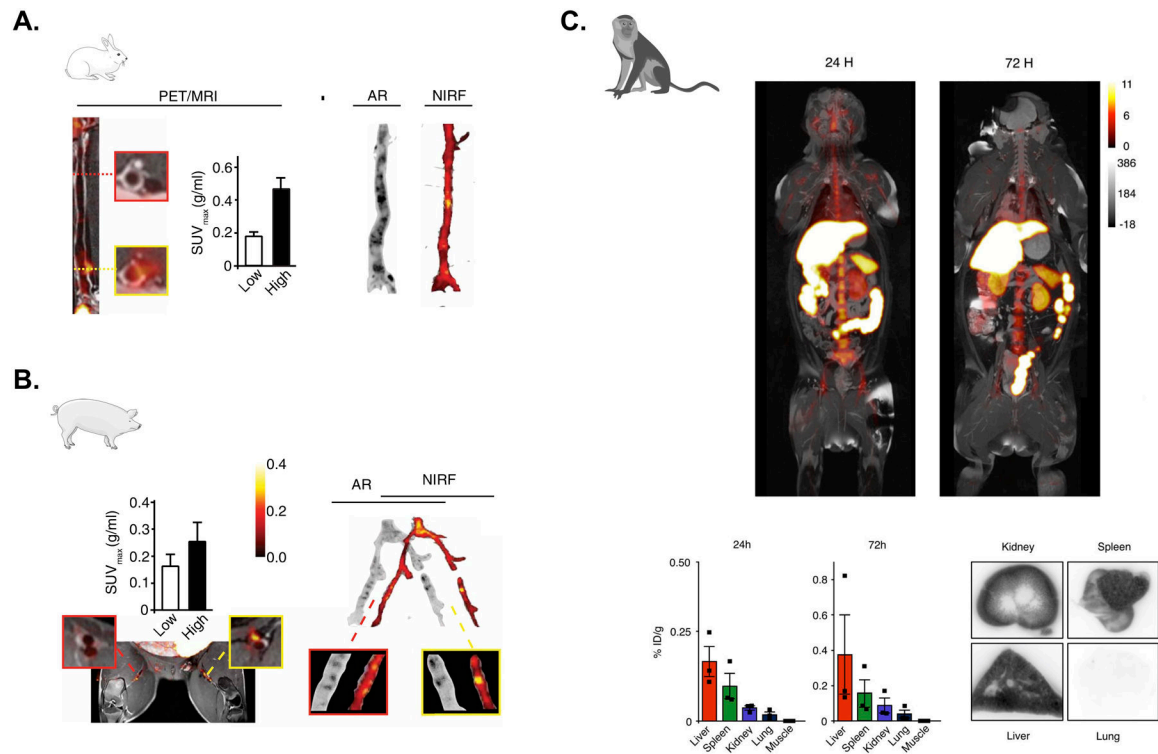


**Figure 3.**

(A) **Left**, PET/MRI assessment of plaque targeting and quantification of standardized uptake values (SUVs) in a representative rabbit 48 hours after injection of  $^{89}\text{Zr}$ -labeled S-HDL. Low and high uptake regions are respectively shown in the red- and yellow-bordered squares. **Right**, the regional distribution of S-HDL in atherosclerotic rabbits is shown by autoradiography (AR;  $^{89}\text{Zr}$ -labeled S-HDL) and near-infrared fluorescence (NIRF; DiD-S-HDL) 48 hours after injection. Adapted from Binderup et al.<sup>49</sup> (B) **Left**, PET/MRI assessment of plaque targeting and quantification of standardized uptake values (SUVs) in a representative pig 48 hours after injection of  $^{89}\text{Zr}$ -labeled S-HDL. Low and high uptake regions are respectively shown in the red- and yellow-bordered squares. **Right**, the regional distribution of S-HDL in atherosclerotic pigs is shown by autoradiography (AR;  $^{89}\text{Zr}$ -labeled S-HDL) and near-infrared fluorescence (NIRF; DiD-S-HDL) 48 hours after injection. Adapted from Binderup et al.<sup>49</sup> (C) Six non-human primates were infused with  $^{89}\text{Zr}$ -labeled TRAF6i-HDL (1 mg/kg). Dynamic PET images were acquired within 60 minutes after infusion. Static PET/MRI scans were performed at 24, 48 and 72 hours. NHP were sacrificed after 72 hours. Organs were collected for ex vivo analysis. Static PET/MR images at 24 and 72 hours show the distribution and accumulation of TRAF6i-HDL (**upper panel**). Gamma counting shows nanoparticle biodistribution in NHPs at 24 and 72 hours post administration of  $^{89}\text{Zr}$ -labeled TRAF6i-HDL (n=3) (**lower panel**). Adapted from Lameijer et al.<sup>50</sup>

**Table 1.**

Comparison of strengths and weaknesses of different imaging modalities. From the Table it can be observed that combined PET/MRI scanners capitalize on the high level of complementarity and synergism of PET and MRI, even more so than combined PET/CT imagers. MRI, magnetic resonance imaging. PET, positron emission tomography. CT, computed tomography.

	<i>MRI</i>	<i>PET</i>	<i>CT</i>
<i>sensitivity</i>	low	high	low
<i>quantification</i>			high
<i>spatial resolution</i>			
<i>tissue characterization</i>			
<i>multi-parametric imaging</i>	high	low	medium
<i>partial volume error correction</i>			
<i>motion correction</i>			low
<i>attenuation correction</i>	low	Na	high

Author Manuscript

Author Manuscript

Author Manuscript

Author Manuscript